# Coherent Foucault imaging: A method for imaging magnetic domain structures in thin films

Cite as: Journal of Applied Physics **76**, 5349 (1994); https://doi.org/10.1063/1.357188 Submitted: 20 April 1994 . Accepted: 19 July 1994 . Published Online: 04 June 1998

J. N. Chapman, A. B. Johnston, and L. J. Heyderman





## **ARTICLES YOU MAY BE INTERESTED IN**

Quantitative imaging of magnetic domain walls in thin films using Lorentz and magnetic force microscopies

Journal of Applied Physics 90, 5220 (2001); https://doi.org/10.1063/1.1412829

Lorentz microscopy of small magnetic structures (invited)

Journal of Applied Physics 85, 5237 (1999); https://doi.org/10.1063/1.369955

Improved Foucault imaging of magnetic domains with a modified 400 kV transmission electron microscope

Review of Scientific Instruments 64, 1038 (1993); https://doi.org/10.1063/1.1144174









## Coherent Foucault imaging: A method for imaging magnetic domain structures in thin films

J. N. Chapman, A. B. Johnston, and L. J. Heyderman Department of Physics and Astronomy, University of Glasgow, Glasgow G12 8QQ, United Kingdom (Received 20 April 1994; accepted for publication 19 July 1994)

A method for imaging magnetic domain structures in the transmission electron microscope is described. Coherent Foucault imaging provides a direct means of producing a magnetic interferogram which reveals the quantitative distribution of magnetic induction across the specimen. The technique requires the high coherence of a field-emission gun system and the ability to position an aperture accurately to cut part of the diffraction pattern. A simple analytical theory, together with computer simulations and experimental results, is presented to demonstrate the power of the technique.

#### I. INTRODUCTION

The Lorentz modes of transmission electron microscopy are widely used for the study of domains and domain wall structures in thin ferromagnetic films. A number of different imaging techniques exist but all have in common the fact that magnetic contrast arises as a result of the small deflections that the electron beam undergoes due to the Lorentz force acting on the moving electrons as they pass through the specimen. Alternatively, the same phenomena can be viewed from a wave-mechanical standpoint in which case the magnetic specimen acts to modulate the phase of the electron wave.<sup>1</sup>

The various experimental techniques in use have been reviewed extensively elsewhere.<sup>2,3</sup> Of those which are normally implemented in a fixed-beam or conventional transmission electron microscope (CTEM), the Fresnel and Foucault modes are the most widely employed. Using Fresnel imaging, domain walls are revealed as narrow bright or dark bands on an otherwise constant background as a result of defocusing the imaging lens. In the Foucault mode, domain contrast is revealed by inserting a blocking aperture in the back focal plane of the imaging lens, thereby preventing some electrons from contributing to the image. The Foucault mode, unlike the Fresnel mode, has marked directional properties and pairs of images with the blocking aperture rotated through 90° are required to obtain a clear picture of the magnetic structure. Between them, the Fresnel and Foucault modes provide information on the overall domain geometry and the direction of magnetization in, at least, the larger domains. However, they are ill suited for providing a quantitative description of the spatial variation of magnetic induction across the specimen and do not readily reveal gradual or subtle changes in magnetization direction.

For these purposes either the differential phase contrast imaging mode<sup>4</sup> or electron holography<sup>5</sup> are more suited. The former uses a scanning transmission electron microscope and is not considered further here. The latter is normally implemented on a fixed-beam instrument but requires an electron biprism to be situated beneath the specimen to interfere electron waves that have passed through the magnetic specimen with those that have passed adjacent to it. An electron hologram is formed in the recording plane of the microscope and

can be reconstructed optically or by computer to reveal a magnetic interferogram which maps lines of force, separated by the flux quantum h/e across the magnetic specimen. While this indeed usually provides all the information required (exceptions being when wall structures themselves are of concern and when the phase shift is very small) it is obtained only after processing the recorded hologram and hence is not as useful as the Fresnel and Foucault modes for rapid surveys or studies of large specimen areas to identify the structures of greatest interest.

The most successful implementations of electron holography have been achieved on microscopes equipped with a small bright electron source such as a field-emission gun (FEG).6 In this article we revisit the Foucault mode and introduce a very significant modification to show that, when practiced on an FEG instrument, it can provide directly magnetic interferograms of the kind discussed above in the context of off-axis electron holography. Indeed, the mode can properly be regarded as a kind of in-line holography and one which is capable of providing a quantitative description of the magnetic induction distribution across a specimen in real time. The basic theory behind the so-called coherent Foucault (CF) imaging is given in Sec. II. Thereafter, computer simulations are presented in Sec. III which confirm the predictions of the simple theory and which demonstrate the stability of the fringe patterns to small variations in the positioning of the aperture. Section IV provides a description of the experimental implementation and presents results from small regular magnetic elements defined by electron-beam lithography. Finally, a brief discussion is given about likely application areas for the new technique.

## II. SIMPLE APPROXIMATE ANALYTICAL THEORY OF COHERENT FOUCAULT IMAGING

To illustrate how a magnetic interferogram is generated by simply inserting an aperture at an appropriate point in a CTEM column we consider a uniformly magnetized semi-infinite thin magnetic film as shown in Fig. 1(a). The specimen transmittance  $f_0(x)$  of such an object is given by

$$f_0(x) = \exp(i\gamma x)H(x) + [1 - H(x)],$$
 (1)

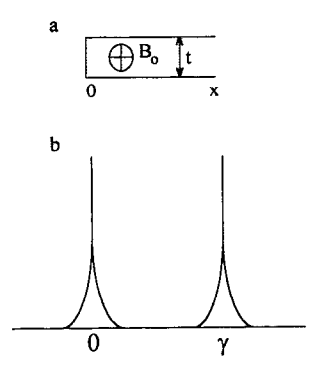


FIG. 1. (a) A semi-infinite uniformly magnetized magnetic thin film; (b) schematic of the corresponding intensity distribution in the diffraction plane.

where H(x) is the Heaviside function equal to unity for x>0 and to zero for x<0 and  $\gamma$  is given by  $2\pi eB_0t/h$ .  $^1B_0$  is the saturation induction of the magnetic material and t is the film thickness. The form of the complex disturbance in the back focal plane of the lens F(k) is given by the Fourier transform of the specimen transmittance and may be written as

$$F(k) = \delta(k)/2 + \delta(k - \gamma)/2 - i/2\pi k + i/2\pi (k - \gamma). \quad (2)$$

The intensity distribution in this plane is shown schematically in Fig. 1(b). If now an aperture of the form H(k) is introduced which removes all negative spatial frequencies, the complex disturbance in the image plane  $f_i(x)$  will differ from that in the object plane. It is straightforward to determine the form of this disturbance numerically but, other than around x=0, the disturbance can be approximated by a simple analytical expression. This is obtained by noting that, provided the aperture just fails to cut the central delta function, the only term in Eq. (2) which is significantly affected is the third term,  $i/2\pi k$ , as none of the others has an appreciable value for k<0. Thus, on application of a second Fourier transform, to move to the image plane we obtain an expression of the form

$$f_i(x) = \exp(i\gamma x)H(x) + \frac{1}{2} - \frac{1}{2}\operatorname{sgn}(x) \otimes [\delta(x)/2 + i/2\pi x],$$
(3)

where  $\otimes$  denotes a convolution and sgn(x) is equal to +1 for x>0 and to -1 for x<0. Equation (3) can be evaluated to yield

$$f_i(x) = \exp(i\gamma x)H(x) + \frac{1}{2} - \frac{1}{4}\operatorname{sgn}(x) - \Delta(x),$$
 (4)

where  $\Delta(x)$  is a function which is strongly peaked about the origin but falls away rapidly on either side of it. Thus, for x<0, the image disturbance assumes a constant value (<1), while for x>0 it is of the form

$$f_i(x) = [\epsilon + \cos(\gamma x)] + i \sin(\gamma x). \tag{5}$$

More precisely, for the example given the constant value in the region x<0 is  $\frac{3}{4}$  while  $\epsilon$  is equal to  $\frac{1}{4}$ . These numerical values change, however, if the aperture is moved slightly to just remove the central delta function, although the generic form remains unaltered under these conditions.

The important observation from the above is that the introduction of the aperture in the back focal plane has re-

sulted in an additional term  $\epsilon$  being present in addition to that directly attributable to the magnetic specimen in the region x>0. Thus, the intensity distribution I(x) in this region is given by

$$I(x) = \mu + \nu \cos(\gamma x), \tag{6}$$

where  $\mu$  and  $\nu$  are constants whose values again depend on the precise positioning of the aperture. We see then that the region occupied by the magnetic specimen consists of a set of interference fringes, running parallel to the induction direction, with a periodicity  $h/eB_0t$ .

As what has been described so far is simply the basic Foucault technique, it is worth asking the question why such fringes are not well known in practice and why the simple analysis performed above has not, to the authors' knowledge, been reported before. The answer to this question is that unless the microscope is equipped with a FEG the source subtends a sufficiently large angle that the visibility of the fringes is reduced to zero. Under these conditions Foucault images just show regions in which differently oriented domains appear with different intensity levels, which is precisely what a classical argument based on beam deflections would predict. We return to a fuller discussion of the experimental conditions that must be fulfilled to see magnetic interferograms in Sec. IV.

Using the technique described so far, it is apparent that information is lost if the specimen is more complex than the very simple example shown in Fig. 1. For example, if it has two domains, oriented along the positive and negative y axes as shown in Fig. 2(a), a problem arises in that electrons passing through the domain with magnetization along the negative y axis will inevitably hit the aperture itself and play no

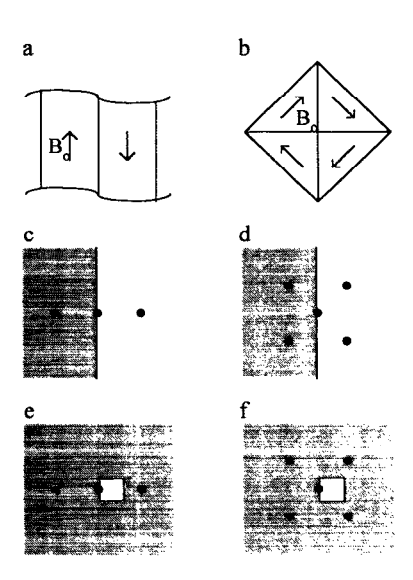


FIG. 2. (a) and (b) simple one- and two-dimensional magnetization distributions suitable for investigating CF imaging; (c) and (d) the corresponding diffraction patterns with a half-plane phase-shifting aperture superposed; (e) and (f) as (c) and (d) but with a phase-shifting aperture containing a single small hole.

further role in the image formation process. This problem can be overcome using a modification to the procedure described above in which the solid aperture is replaced by an electron transparent phase-shifting aperture, such as a thin foil of uniform thickness containing a hole. Furthermore, we note that the phase shift  $\Phi$  is given by

$$\Phi = \pi V T / \lambda E, \tag{7}$$

where V is the mean inner potential of the phase-shifting film, T is its thickness, and  $\lambda$  and E are the wavelength and energy of the electron beam, respectively. Thus, by varying the thickness of the film the magnitude of the phase shift can be selected by the experimenter.

If the magnitude of the phase shift is chosen to be  $\pi$  radian, the effect of a half-plane aperture is to multiply the disturbance in the back focal plane by sgn(k). For a specimen of the form shown in Fig. 1 the complex disturbance in the image plane, equivalent to Eq. (3), is

$$f_i(x) = \exp(i\gamma x)H(x) + \frac{1}{2} - \frac{1}{2}\operatorname{sgn}(x) \otimes (i/\pi x), \tag{8}$$

which can be written in the form

$$f_i(x) = \exp(i\gamma x)H(x) + \frac{1}{2} - 2\Delta(x). \tag{9}$$

It follows, then, that Eq. (6) still holds, albeit with different values for the constants  $\mu$  and  $\nu$ . Thus, a magnetic interferogram with fringes of the same spacing is again formed and, in this instance, the amplitude of the disturbance everywhere in the back focal plane has been unaffected. The advantage of a phase-shifting aperture becomes clear when we consider a one-dimensional object of the form shown in Fig. 2(a) or more general two-dimensional magnetization distributions. A simple example of the latter, which relates to the experimental results detailed in Sec. IV, is shown in Fig. 2(b).

To gain insight into the kind of effects we might expect, we consider a magnetic specimen of finite extent defined by a shape function  $s(\mathbf{r})$  where  $\mathbf{r}$  is a two-dimensional vector and  $s(\mathbf{r})$  assumes a value of unity within the specimen and zero outside it. With the usual assumption that the magnetic specimen modulates only the phase of the electron wave  $\varphi(\mathbf{r})$ , the specimen transmittance can be written as

$$f_0(\mathbf{r}) = \exp[i\phi(\mathbf{r})]s(\mathbf{r}) + [1 - s(\mathbf{r})], \tag{10}$$

and the disturbance in the back focal plane is of the form

$$F(\mathbf{k}) = \Psi(\mathbf{k}) \otimes S(\mathbf{k}) + \delta(\mathbf{k}) - S(\mathbf{k}). \tag{11}$$

Here  $\Psi(\mathbf{k})$  and  $S(\mathbf{k})$  are the Fourier transforms of  $\exp[i\varphi(\mathbf{r})]$  and  $s(\mathbf{r})$ , respectively. It is important to note that for most magnetic specimens the first term generally makes no significant contribution in the vicinity of  $\mathbf{k}=0$  and that, for specimens in which the magnetization is principally oriented along a small number of directions, there are many radial directions in  $\mathbf{k}$  space along which the contribution from the first term is negligible. We now insert a half-plane aperture introducing a phase shift of  $\pi$  so that the edge of the film just misses the central delta function and lies along one of these directions, denoted by  $k_x$ . Under these conditions, individual regions where  $\Psi(\mathbf{k}) \otimes S(\mathbf{k})$  is appreciable are either unaffected or suffer in their entirety a phase change of  $\pi$ . Hence, the only term that it is significantly affected by the insertion

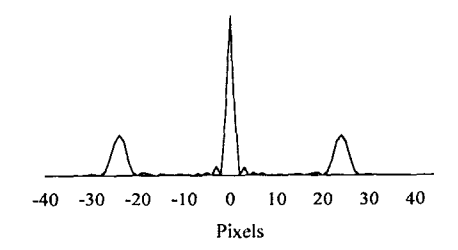


FIG. 3. The diffraction pattern from the object shown in Fig. 2(a).

of the film is  $S(\mathbf{k})$  which must be replaced by  $S(\mathbf{k})\operatorname{sgn}(k_x)$ . This is illustrated schematically for both the magnetization distributions of Figs. 2(a) and 2(b) in Figs. 2(c) and 2(d), respectively.

Moving to the image plane the complex disturbance takes the form

$$f_i(\mathbf{r}) = \exp[i\varphi(\mathbf{r})]s(\mathbf{r}) + 1 - s(\mathbf{r}) \otimes i/\pi x [\delta(y)]. \tag{12}$$

The last term is strongly peaked around the edges of the specimen and if its effect can be ignored elsewhere, it is clear that, once again, strong fringes are formed within the magnetic sample as a result of a mixing of the first two terms within its boundaries.

So far the phase-shifting aperture has been assumed to be in the form of a semi-infinite half-plane. In practice an approximation to this can be realized by using the edge of a film or a sufficiently large hole whose dimensions appreciably exceed those of the magnetic diffraction pattern itself. A variation on this is realized if a hole whose size is small compared with that of the magnetic diffraction pattern is positioned as shown in Figs. 2(e) and 2(f). Under these conditions all magnetic spots suffer the phase shift  $\Phi$  as all of them pass through the thin film aperture. This contrasts with the case already considered where some magnetic spots are phase shifted while others are not. In both cases, the only part of the diffraction pattern that undergoes a differential phase shift is that part very close to the center and the analysis given above is broadly applicable to both cases. Differences that arise according to the form of aperture used are discussed in the following section.

## III. COMPUTER MODELING OF COHERENT FOUCAULT IMAGES

To explore the detailed form of the intensity variation in a CF image computer modeling has been used. The object is represented by a one- or two-dimensional complex array of 512 or  $(512)^2$  points. Typically the magnetic object occupies the central portion of the array and is surrounded by free space. To illustrate the effect of various apertures we consider an object of the form shown in Fig. 2(a). For subsequent comparison with experimental results the magnetic material is assumed to be a permalloy film with a saturation induction of 1 T and a thickness of 50 nm. The width of each domain is taken as  $0.5 \, \mu \text{m}$  and the total window size is  $2.0 \, \mu \text{m}$ . The diffraction pattern corresponding to the object is obtained using a fast Fourier transform and its intensity distribution is shown in Fig. 3. It can be seen that the pattern

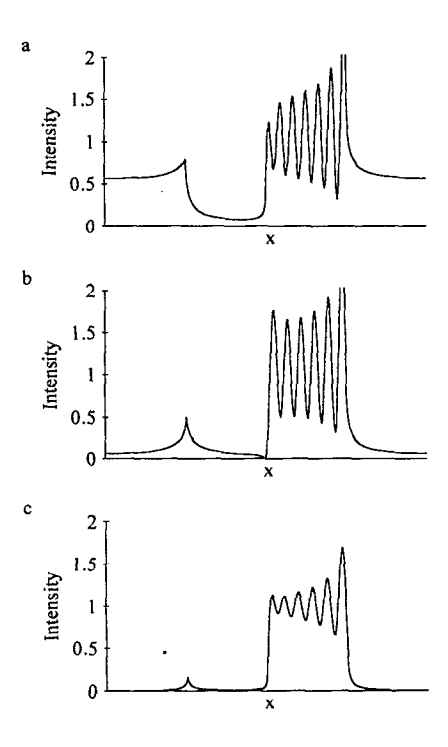


FIG. 4. Calculated CF images of the object shown in Fig. 2(a) obtained using an opaque half-plane aperture; images (a), (b), and (c) show the effect of moving the edge of the aperture in single-pixel steps across the center of the diffraction pattern.

consists of three prominent lobes with relatively low intensity values in between. The spatial frequencies at which the magnetic contributions assume their maximum values are ±0.012 nm<sup>-1</sup> and they are separated from the central spike (arising from the free space surrounding the specimen) by 24 pixels. This is sufficient to allow the aperture edge to be located with at least as high a precision as can be achieved experimentally. Apertures themselves are chosen to be of the opaque half-plane, phase-shifting half-plane, or phase shifting small hole kind. The magnitude of the phase shift can be varied, as can the size of the hole for the last-named variant. Thereafter, the aperture edge position is specified with respect to the diffraction pattern, the complex distribution modified appropriately, a second Fourier transform performed, and the square modulus of the resulting distribution displayed to yield a CF image. In a typical sequence a number of aperture positions are specified and the resulting images provide information over what range of aperture locations magnetic interferograms are observed and the stability of the fringe pattern to small variations in aperture position. A fuller description of these and the artefacts that arise from an incorrectly positioned aperture is in preparation<sup>7</sup> while below we show results with the aperture near optimally positioned to confirm the predictions of the simple analytical approach of Sec. II.

Figure 4 shows what happens as an opaque aperture is moved at single-step  $(0.5~\mu m^{-1})$  intervals from one side of the sharp central maximum to the other. In all cases fringes are clearly seen in one domain while near zero intensity is present in the other. The fringe width is not completely constant but varies by <10% as the aperture moves from one

side of the central maximum to the other. Movement of the aperture edge further from the central position leads to images displaying fringes of the same form but reduced visibility.

The effect of replacing the opaque aperture by an identically located half-plane aperture introducing a phase shift of  $\pi$  radian is seen in Fig. 5. Fringes of similar spacing and comparable visibility are now present in both domains. Furthermore, the total number of fringes present across the specimen remains constant at 13 as the aperture is moved across the central spot. Note that at the center of the fringe pattern there is a near discontinuity which results from the fact that electrons passing through only one domain suffer a phase shift due to the aperture in the back focal plane. This is not the case when a phase-shifting aperture containing a small hole is used. Some results for this case are shown in Fig. 6. Here one edge of the hole is held in its optimal position (where it cuts the center of the diffraction pattern) while the size of the hole is varied. In Fig. 6(a) the hole is unrealistically small with a size of 2-step intervals  $(1 \mu m^{-1})$  while in the remaining figures its size is increased to 6 and 10 units. Thus the largest hole extends  $\sim 40\%$  of the distance to one of the magnetic peaks in the diffraction pattern and this is comparable with the apertures used to obtain the experimental results detailed in the following section. Figure 6 shows, once again, that apart from a modest variation in fringe visibility the coherent Foucault image is very stable to the kind of changes in imaging conditions that will inevitably

Under the various imaging conditions used in Figs. 5 and 6 the fringe spacing varies by less than 10% about a mean value of 80 nm. This compares favourably with  $h/eB_0t$  (as

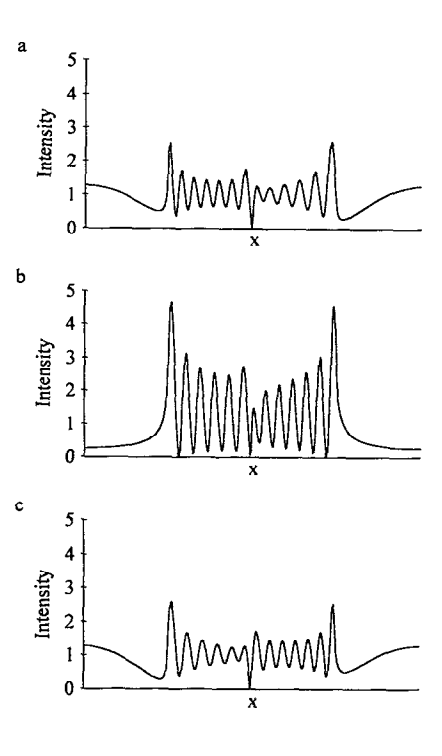


FIG. 5. As Fig. 4 but using a phase-shifting half-plane aperture.

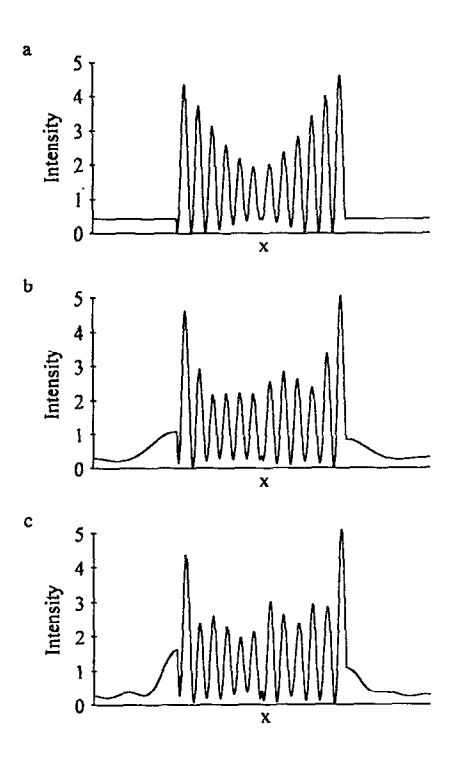


FIG. 6. Calculated CF images using a phase shifting aperture containing a small hole, the hole being positioned asymmetrically so that one edge cuts the center of the diffraction pattern. The sizes of the hole in (a), (b), and (c) are 2, 6, and 10 pixel units, respectively.

predicted by the simple theory of Sec. II) which for the magnetic parameters used in the simulation evaluates to 82.5 nm.

## IV. EXPERIMENTAL COHERENT FOUCAULT IMAGING

We have demonstrated coherent Foucault imaging using a modified Philips CM20 FEG TEM to obtain magnetic interferograms of small permalloy elements fabricated by electron beam lithographic and evaporation techniques. Individual elements (with magnetic induction and thickness as described in the previous section) are rectangular in shape with dimensions between 0.2 and 4.0  $\mu$ m. Their study provides insight into the effect of shape and size on magnetic properties and they form a near-ideal micromagnetic model system. Furthermore, their dimensions are comparable to what might be expected for the next generation of pole-tip regions of recording heads and magnetoresistive sensors in ultrahigh density recording systems.

The principal modifications to the TEM relevant to the work described here are the inclusion of two additional super mini-lenses sited above and below the main objective lens. These so-called Lorentz lenses are nonimmersion lenses and allow high quality images to be obtained while the specimen remains in magnetic field-free space. Using these lenses, suitably excited, it is possible to accurately locate the diffraction pattern in the relevant aperture plane while images can be seen either on the microscope viewing screen or, through the use of a low-light-level TV pickup system, on a TV monitor. The latter is recommended as it facilitates the accurate final positioning of the aperture which is done by maximizing the visibility of the fringes in the image.

The opaque aperture used to obtain the experimental images was simply a standard TEM aperture with a large hole. In practice the edges of such apertures are neither completely abrupt nor uniform but, with care, regions suitable for blocking part of the magnetic diffraction pattern could be found. Phase-shifting apertures were fabricated by ion-beam milling small holes in a silicon nitride membrane supported on a robust silicon substrate containing a central window. Holes significantly larger than the extent of the magnetic diffraction pattern were used as approximations for half-plane phaseshifting apertures while holes ≤1 µm in diameter were needed when the phase shift was to be applied to the central portion of the diffraction pattern alone. In practice a number of holes of varying size were etched in the same membrane to accommodate different experimental investigations. It should be noted that in the most suitable plane for locating apertures in our instrument the distance between a magnetic diffraction spot and the central spot is  $\approx 3 \mu m$  for 50-nmthick permalloy elements.

As the silicon nitride was in the form of a uniform amorphous thin film and ion-beam milling allowed regular shaped sharp edged holes to be introduced, the phase-shifting apertures were in many ways more satisfactory than their opaque counterparts. However, one problem that remained was the appropriate thickness to ensure a phase shift of  $\pi$  radian. Equation (7) shows how this depends on both the film thickness and the mean inner potential. Unfortunately, the authors are unaware of any measurement of the latter quantity in the literature. Guided by measured values for similar materials 10,11 a value of 10 eV was assumed. With this value, a film thickness of 50 nm, and an electron energy of 200 keV, a phase shift very close to  $\pi$  radian is predicted. Furthermore, computer simulation suggests that differences introduced due to small departures from  $\pi$  radian are very small suggesting that a precise knowledge of inner potential is not reauired.

Figure 7 shows coherent Foucault images of a permalloy element with dimensions  $3\times1~\mu\text{m}^2$ . As predicted, fringes are present in only some of the domains when the opaque aperture is used. Furthermore, a small amount of blurring is visible close to the boundaries between those domains where fringes can be seen and those which appear simply as regions of low intensity. This is a result of a lack of abruptness and consequent incomplete opacity at the aperture edge. The lower image in Fig. 7 shows the advantages of using a phase shifting aperture. High-visibility fringes are apparent across the magnetic element as a whole and give a direct and immediate picture of the spatial variation of induction. This is shown schematically in Fig. 8 and consists of a solenoidal distribution comprising three flux closure circuits within the element. The number three is determined by the aspect ratio of the element under investigation.

Figure 9 provides other examples of coherent Foucault images, both recorded with the small hole phase-shifting aperture, to show the kind of information that is accessible when more complex magnetic structures are studied. In the upper part of Fig. 9, a somewhat different solenoidal magne-

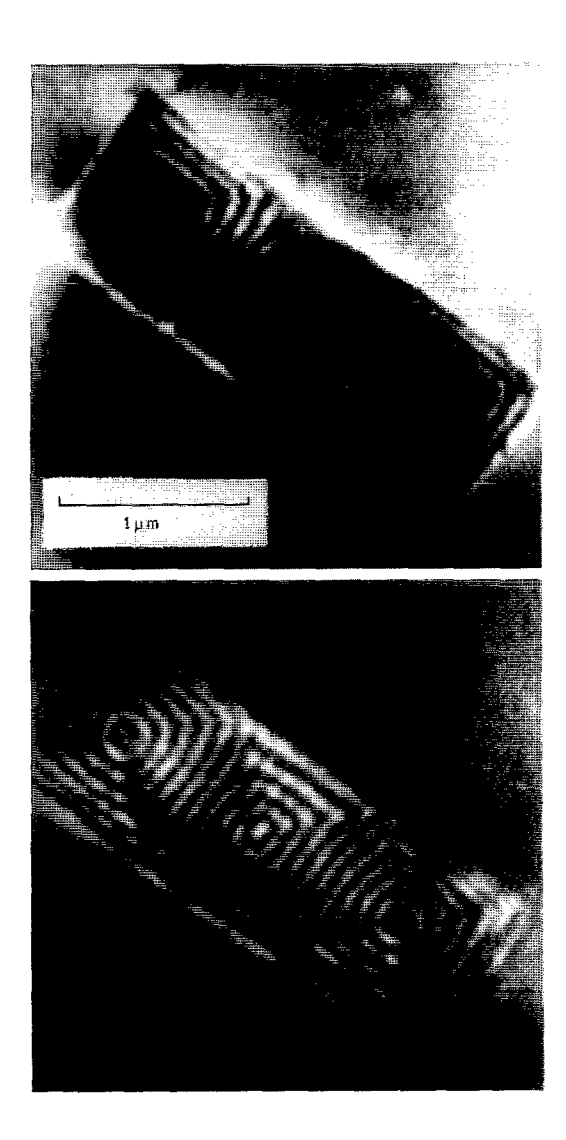


FIG. 7. CF images of a Permalloy element using an opaque aperture and a phase-shifting aperture containing a small hole.

tization distribution is seen in a more elongated element. Here, the central portion of the element contains a 180° wall and, as expected for a permalloy film of 50 nm thickness, this is of the cross-tie type. The interferogram provides an immediate and vivid picture of the near continuous variation of magnetization direction close to the wall but also shows how, near the edge, the magnetization once again lies parallel to the element axis to avoid the creation of surface magnetic charge. What happens when one of the dimensions of an element is reduced sufficiently to preclude complete flux closure is shown in the lower part of Fig. 9. The resulting non-

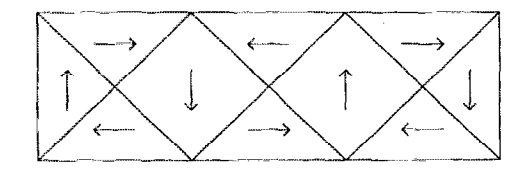


FIG. 8. Schematic of the magnetization distribution of the element shown in Fig. 7.



FIG. 9. CF images of Permalloy elements supporting more complex magnetization distributions,

solenoidal magnetization distribution has a particularly complex variation close to the ends of the element; however, the attempt to introduce a degree of flux closure and the consequent reduction of surface magnetic charge on the end faces of the element can be seen clearly in the coherent Foucault image. Using other Lorentz microscopy techniques this information is either more time consuming or, indeed, impossible to obtain.

## V. CONCLUSIONS

We have shown that, by taking advantage of the very small source size available from a field-emission gun, the well established Foucault imaging technique can be developed to yield additional quantitative information that is not readily accessible using the other modes of Lorentz microscopy in frequent use. The resulting images can be thought of as magnetic interferograms (or in-line holograms) and closely resemble those obtained using off-axis holography. However, an important advantage of the Foucault technique is that the fringes can be clearly seen on the viewing screen or on a TV monitor in real time so that useful information is available directly and without any processing whatsoever. Of particular value, using techniques of this kind, is access to a direct measure of the flux linked along an electron trajectory

as well as the overall form of its spatial variation. The former information is determined from the spacing of the interference fringes.

We are particularly encouraged by the robustness of the magnetic interferograms themselves. Theoretical simulations have shown that they are relatively insensitive to small variations in imaging conditions and our practical experience is that once a phase-shifting aperture has been accurately located the system is very stable. Furthermore, no problems have been encountered to date with either damage to the aperture or a buildup of contamination on its edge. This suggests that the imaging mode will be of use for extensive investigations involving a large number of magnetic elements or *in situ* experiments involving, for example, the effect of temperature variation on the domain structure.

#### **ACKNOWLEDGMENTS**

We would like to thank L. Zhou for provision of the specimen containing the magnetic elements, Professor C. D. W. Wilkinson for provision of the lithographic facilities

where the specimen and the phase-shifting aperture were fabricated, and Dr. B. Bormans for his advice in operation of the microscope. We also gratefully acknowledge financial support from the SERC and the University of Glasgow.

- <sup>1</sup>Y. Aharonov and D. Bohm, Phys. Rev. 115, 485 (1959).
- <sup>2</sup>J. N. Chapman, J. Phys. D. Appl. Phys. 17, 623 (1984).
- <sup>3</sup>I. R. McFadyen and J. N. Chapman, EMSA Bull. 22, 64 (1992).
- <sup>4</sup>J. N. Chapman, I. R. McFadyen, and S. McVitie, IEEE Trans. Magn. MAG-26, 1506 (1990).
- <sup>5</sup>A. Tonomura, Rev. Mod. Phys. **59**, 639 (1987).
- <sup>6</sup> A. Tonomura, T. Matsuda, H. Tanabe, N. Osakabe, J. Endo, A. Fukuhara, K. Shinagawa, and H. Fujiwara, Phys. Rev. B 25, 6799 (1982).
- <sup>7</sup>A. B. Johnston and J. N. Chapman (unpublished).
- 8 S. McVitie and J. N. Chapman, IEEE Trans. Magn. MAG-24, 1778 (1988).
- <sup>9</sup>J. N. Chapman, R. P. Ferrier, L. J. Heyderman, S. McVitie, W. A. P. Nicholson, and B. Bormans, in *Electron Microscopy and Analysis*, edited by A. J. Craven (IOP, Bristol, 1993), p. 1.
- <sup>10</sup> M. Gajdardzidka-Josifovska, M. R. McCartney, W. J. de Ruijter, D. J. Smith, J. K. Weiss, and J. M. Zuo, Ultramicroscopy 50, 285 (1993).
- <sup>11</sup> J. K. Weiss, W. J. de Ruijter, M. Gajdardziska-Josifovska, M. R. McCartney, and D. J. Smith, Ultramicroscopy 50, 301 (1993).